Distributed State Estimation in Digital Distribution Networks Based on Proximal Atomic Coordination

Zhelin Liu, Shiyuan Gao, Peng Li, *Senior Member*, *IEEE*, Haoran Ji, *Member*, *IEEE*, Wei Xi, Hao Yu, *Member*, *IEEE*, Jianzhong Wu, *Member*, *IEEE*, Chengshan Wang, *Senior Member*, *IEEE*

***Abstract*—With the emerging digitalization technologies represented by edge computing, distribution networks are gradually transforming into digital distribution networks (DDNs). The realization of edge computing drives the distributed operation of DDNs, where multiple areas exchange boundary information through edge computing devices. Benefitting from the data acquisition and computing capacity of edge computing devices, it is feasible to perform accurate and real-time state estimation on the edge side. Aiming at the state perception with edge computing devices in DDNs, this paper proposes a distributed state estimation (DSE) method based on the proximal atomic coordination (PAC) algorithm. Firstly, based on convex relaxation optimization, the state estimation model is converted into a positive semidefinite programming model to solve the nonconvexity caused by nonlinear measurements, which ensures the accuracy and convergence of state estimation. Then, a DSE method based on the PAC algorithm is proposed to exchange information of each area, which reduces the computation time and realizes the efficient state estimation on the edge side. The model and the effectiveness of the proposed method are numerically demonstrated on the modified PG&E 69-node system and the test case from a practical pilot in Guangzhou, China.**

***Index Terms*—digital distribution networks (DDNs), distributed state estimation (DSE), semidefinite programming (SDP), proximal atomic coordination (PAC).**

NOMENCLATURE

Sets	
$\mathcal{N}$	Set of all nodes in DDNs
$\mathcal{L}$	Set of all lines in DDNs
$\mathcal{N}_i$	Set of nodes connected to node i
Indices	
i, j	Index of nodes
ij	Index of lines
k	Index of areas
n	Index of SCADA and AMI measurements
r	Index of D-PMU measurements
l	Index of zero injection nodes
Variables	
$\boldsymbol{v}$	Nodal complex voltage
$\boldsymbol{z}$	Measurement value
$\boldsymbol{e}$	Measurement error
$\boldsymbol{R}$	Measurement error covariance matrix
σ_n	Standard deviation of the n-th measurement
v_i	Nodal voltage magnitude at node i
$\boldsymbol{V}$	Complex voltage outer product
$\boldsymbol{\zeta}$	Measurement values of D-PMU
$\boldsymbol{\chi}$	Auxiliary variable for state estimation
$\boldsymbol{\mu}_k, \boldsymbol{\nu}_k$	Primal variables of area k
$\hat{\boldsymbol{\mu}}_k, \hat{\boldsymbol{\nu}}_k$	Dual variables of area k
Parameters	
N	Number of all nodes
Z	Number of zero injection nodes
S	Number of SCADA and AMI measurements
P	Number of D-PMU measurements
M	Number of multi-source measurements, $M = S + P$
K	Number of areas
y_{ij}	Admittance of line ij
b_{ij}^{shunt}	Shunt susceptance of line ij
$\boldsymbol{Y}$	Nodal admittance matrix
$\boldsymbol{Y}_i$	Admittance matrix related to node i
$\boldsymbol{Y}_{ij}$	Admittance matrix related to line ij
$\boldsymbol{H}_i^{\text{P}}, \boldsymbol{H}_i^{\text{Q}}$	Active and reactive power injection measurement matrix at node i
$\boldsymbol{H}_{ij}^{\text{P}}, \boldsymbol{H}_{ij}^{\text{Q}}$	Active and reactive power measurement matrix of line ij
$\boldsymbol{H}_i^{\text{V}}$	Voltage magnitude measurement matrix at node i
$\boldsymbol{H}_{ij}^{\text{I}}$	Line current magnitude measurement matrix of line ij
$\boldsymbol{H}_i^{\text{PMU}}$	Voltage phasor measurement matrix of D-PMU at node i
$\boldsymbol{H}_{ij}^{\text{PMU}}$	Line current phasor measurement matrix of D-PMU of line ij
ω	Rank of voltage outer product
$\widetilde{\boldsymbol{D}}_k$	Internal constraints of area k
$\boldsymbol{J}_k$	Coordination matrix of area k
τ	Iteration step
ε	Predefined iteration tolerance

This work was supported by the National Key R&D Program of China (2020YFB0906000, 2020YFB0906001). *(Corresponding author: Peng Li.)*

Z. Liu, S. Gao, P. Li, H. Ji, H. Yu, and C. Wang are with the Key Laboratory of Smart Grid of Ministry of Education, Tianjin University, Tianjin 300072, China (email: liuzhelin@tju.edu.cn; gaosy@tju.edu.cn; lip@tju.edu.cn; jihaoran@tju.edu.cn; tjuyh@tju.edu.cn; cswang@tju.edu.cn).

W. Xi is with the Digital Grid Research Institute of China Southern Power Grid, Guangzhou 510670, Guangdong Province, China (email: xiwei@csg.cn).

J. Wu is with the Institute of Energy, School of Engineering, Cardiff University, Cardiff CF24 3AA, U.K. (email: wuj5@cardiff.ac.uk).

I. INTRODUCTION

WITH the development of advanced digitalization technologies including sensor measurements and edge computing, traditional distribution networks are transforming into digital distribution networks (DDNs) [1], [2]. To reduce the data transmission burden caused by massive sensor meas-

urements, edge computing devices integrating the functions of data acquisition, storage, computing, and control are introduced [3], [4]. Compared with conventional centralized operation, the capacities on local monitoring, dispatching, and regulation of edge computing devices make the distributed operation convenient and feasible in DDNs.

Benefitting from the data acquisition and computing, accurate distributed state estimation (DSE) based on edge computing devices in realizing the monitoring and operation of DDNs is becoming a trend [5], [6]. The edge computing devices gather multi-source measurements from sensing terminals. The multi-source measurements in DDNs may consist of conventional supervisory control and data acquisition (SCADA), advanced metering infrastructure (AMI), and novel distribution phasor measurement unit (D-PMU) [7], [8]. The differences in time scale and accuracy among these multi-source measurements pose challenges for the reliable convergence of state estimation. On the other hand, with the high penetration of distributed generators (DGs) [9], [10], the variability and uncertainty of DDNs drive the demand for the real-time tracking of operating states more essentially [11]. Thus, the fast convergence of DSE with multi-source measurements is the main concern for the state estimation problem in DDNs.

Owing to the introduction of edge computing devices, the studies on state estimation in DDNs no longer treat the network as a whole but divides it into multiple areas. The existing literatures focusing on the multi-area state estimation can be summarized as hierarchical state estimation and distributed state estimation. As for the hierarchical state estimation, there exists a central coordinator which exploits the results of the local estimators. Ref. [12] proposed a two-step estimator where the results of local estimators were transferred to the central coordinator, and then the voltage profile of the whole network was obtained. Ref. [13] decomposed the nonlinear state estimation process into the mode of local side and coordinator side, which effectively reduced the amount of data transmission and improved the computational efficiency of state estimation. Different from the hierarchical architecture, distributed state estimation is achieved through the cooperation of multiple sub-area estimators without a central coordinator. Ref. [14] proposed a distributed robust state estimation method based on the alternating direction multiplier method (ADMM), which obtained similar results to the centralized state estimation. However, the amount of information exchanged by the multi-area is relatively challenging. Refs. [15] and [16] proposed distributed state estimation methods based on a linearized power flow model and weighted least squares (WLS). The authors in [17] analyzed the impact brought by possible measurements shared among different areas, which drove the design of a new efficient WLS formulation and improved estimation accuracy. Ref. [18] proposed a multi-area estimator based on the overlapping zone approach, which executes local area state estimation after each data exchange with the adjacent areas.

In addition to the estimation accuracy and computation speed, the convergence of state estimation with edge computing devices should also be considered. To realize the fast convergence of state estimation, Gauss-Newton iterative method [19] is widely applied. Since the inherent nonconvexity in state estimation problem, the solution may fall into the local optimum and exist convergence issues [20]. Moreover, the basic WLS estimator gives a larger weight to the zero injection constraints, and the significant difference in weight leads to the "ill-conditioned" gain matrix, resulting in the poor convergence of state estimation [21].

Further considering that the computing resources of edge computing devices are limited, it is essential to reduce the complexity of distributed algorithms. To reduce the amount of data interaction, Ref. [22] proposed a novel distributed convex optimization framework of proximal atomic coordination (PAC). It could achieve linear convergence when the objective function is convex, which showed great potential in computational efficiency. Ref. [23] further proposed a retail market based on the PAC algorithm for optimally managing and scheduling distributed energy resources, which reduced local computational effort and enhanced privacy. Therefore, this paper proposes a PAC algorithm-based distributed state estimation method in DDNs. Firstly, the state estimation model is convexly relaxed for the multi-source measurements in each area and converted into a semidefinite programming (SDP) [24] model to solve the nonconvexity caused by nonlinear measurements, which can ensure the convergence of state estimation. The coordination between multiple areas is implemented with the PAC algorithm to ensure the efficient and accurate solution of the distributed state estimation in DDNs.

The distributed state estimation framework of DDNs is shown in Fig. 1. In the sensing measurement layer, the sensing terminals collect multi-source measurements from SCADA, AMI, and D-PMU. Once the multi-source measurements are obtained, the sensing terminals transmit them to the edge computing layer by communication networks, such as wired optical fiber and wireless 5G, to support advanced applications including state estimation with edge computing devices. The edge computing layer provides a targeted solution for the acquisition and utilization of collected measurements. The edge computing device performs state estimation and exchanges information with other edge computing devices based on the PAC algorithm and lays a more flexible operation foundation for large-scale DDNs.

The contributions of this paper are summarized as follows:

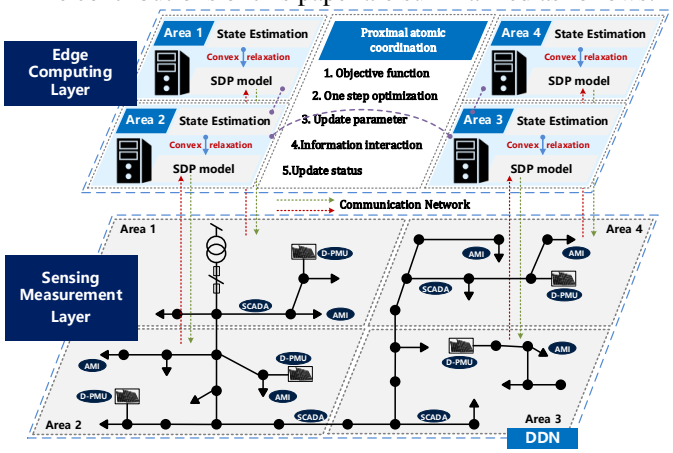

Fig. 1. Distributed state estimation framework of DDNs.

1) To reduce the computational complexity of state estimation with edge computing devices, an efficient DSE method based on the PAC algorithm is proposed. Each area carries out local state estimation independently and interacts boundary information with its neighbors. Compared with the ADMM algorithm, the PAC algorithm exhibits a strictly sublinear convergence in iteration complexity, which results in better estimation accuracy and computational efficiency, and shows the potential for deployment in edge computing devices.

2) In each area, an SDP-based state estimation model considering the multi-source measurements in DDNs is improved. Based on convex relaxation optimization, the state estimation model is transformed into an SDP model, which integrates the nonlinear conventional measurements and the linear D-PMU measurements. It guarantees the effectiveness and convergence of the state estimation in DDNs.

The remaining parts of this paper are organized as follows. Section II introduces the SDP-based state estimation modeling of DDNs. In Section III, a distributed state estimation method based on the PAC algorithm is proposed. Case studies and analysis are given in Section IV. The conclusion is drawn in Section V.

II. SDP-Based State Estimation of Digital Distribution Networks

Considering the multi-source measurements collected by sensing terminals of edge computing devices, the state estimation model is converted into an SDP model based on convex relaxation optimization.

A. Formulation of State Estimation Problem

Consider a distribution network $\{\mathcal{N}, \mathcal{L}\}$, nodes denoted by the set $\mathcal{N} \coloneqq \{1,2,\dots,N\}$ and lines denoted by the set $\mathcal{L} \coloneqq \{\mathcal{L}_{ij} | i,j \in \mathcal{N}\}$. Generally, the voltages $\boldsymbol{v} \coloneqq \{v_i \angle \theta_i | i \in \mathcal{N}\}$ of all nodes in the networks are selected as the state variables. The mathematical relationship of state estimation is described as

$$\boldsymbol{z} = \boldsymbol{h}(\boldsymbol{v}) + \boldsymbol{e} \tag{1}$$

where $\boldsymbol{h}(\boldsymbol{v}) = [h_1(\boldsymbol{v}); h_2(\boldsymbol{v}); \dots; h_M(\boldsymbol{v})]$ is the nonlinear function of measurements $\boldsymbol{z}$ with respect to voltage $\boldsymbol{v}$. The measurement error covariance matrix $\boldsymbol{R}$ can be expressed as $\boldsymbol{R} = \mathrm{cov}(\boldsymbol{e}) = \mathrm{diag}\{\sigma_1^2, \dots \sigma_n^2, \dots, \sigma_M^2\}$.

The multi-source measurements collected by sensing terminals are typically as follows: 1) Real-time measurements, including the conventional SCADA and novel D-PMU measurements. 2) Pseudo measurements, which are constructed from AMI data or load forecasting data. 3) Virtual measurements, which consist of zero power injections at the switching station nodes. In addition, the DGs are equivalent to the power injection at the associated nodes. In this paper, we adopt the AC power flow model [25] to describe the nonlinear function $\boldsymbol{h}(\boldsymbol{v})$.

$$P_i + \mathrm{j}Q_i = v_i \sum_{j \epsilon \mathcal{N}_i} \left(y_{ij} v_j\right)^* \tag{2}$$

where P_i and Q_i are the active and reactive power injection at node i, respectively; $(\cdot)^*$ denotes the conjugate of element "$\cdot$".

Based on the WLS objective function, considering the multi-source measurements and zero injection constraints of DDNs, the state estimation model is described as

$$f(\boldsymbol{v}) = \min_{\boldsymbol{v}} [\boldsymbol{z} - \boldsymbol{h}(\boldsymbol{v})]^{\mathrm{T}} \boldsymbol{R}^{-1} [\boldsymbol{z} - \boldsymbol{h}(\boldsymbol{v})] \tag{3a}$$

$$\mathrm{s.t.}\ \boldsymbol{c}(\boldsymbol{v}) = \boldsymbol{0} \tag{3b}$$

where $\boldsymbol{c}(\boldsymbol{v}) = [c_1(\boldsymbol{v}); c_2(\boldsymbol{v}); \dots; c_Z(\boldsymbol{v})]$ is the zero injection constraints; $(\cdot)^{\mathrm{T}}$ denotes the transposition of element "$\cdot$". Model (3) is usually solved by Gauss-Newton method, which can converge quickly, while is with some limitations: 1) The method is sensitive to the initial value, and it is difficult to converge to the global optimum if the initial value is improperly selected [26]. 2) Due to the existence of zero injection constraints, when the node injection power is relatively larger than other nodes of the networks, it will bring numerical stability issues and deteriorate the convergence [27].

B. SDP-based State Estimation

With the AC power flow model, the multi-source measurements are nonlinearly related to the state variables, which leads to the nonlinearity of the objective function. Ref. [24] constructs the linear relationship of the conventional SCADA and AMI measurements with respect to the state variables based on convex relaxation method, then model (3) is transformed into an SDP model. Similarly, the complex voltages of all nodes are selected as the state variables in this paper, and the voltage outer product is defined as follows.

$$\boldsymbol{V} = \boldsymbol{v}\boldsymbol{v}^{\mathrm{H}} = \begin{bmatrix} \boldsymbol{v}_1 \boldsymbol{v}_1^* & \cdots & \boldsymbol{v}_1 \boldsymbol{v}_N^* \\ \vdots & \ddots & \vdots \\ \boldsymbol{v}_N \boldsymbol{v}_1^* & \cdots & \boldsymbol{v}_N \boldsymbol{v}_N^* \end{bmatrix} \tag{4}$$

where $(\cdot)^{\mathrm{H}}$ denotes the complex-conjugate transposition of element "$\cdot$".

To reformulate all types of measurements $\boldsymbol{z}$ linearly with respect to $\boldsymbol{V}$, admittance matrices are defined firstly.

$$\begin{aligned} \boldsymbol{Y}_i &= \boldsymbol{\xi}_i \boldsymbol{\xi}_i^{\mathrm{T}} \boldsymbol{Y} \\ \boldsymbol{Y}_{ij} &= \left(b_{ij}^{\mathrm{shunt}} + y_{ij}\right) \boldsymbol{\xi}_i \boldsymbol{\xi}_i^{\mathrm{T}} - y_{ij} \boldsymbol{\xi}_i \boldsymbol{\xi}_j^{\mathrm{T}} \end{aligned} \tag{5}$$

where $\{\boldsymbol{\xi}_i | i = 1,2,\dots,N\}$ is the standard basis in N-dimensional space. The measurement matrices of SCADA and AMI measurements are defined as follows.

$$\boldsymbol{H}_i^{\mathrm{P}} = \frac{1}{2}\left(\boldsymbol{Y}_i + \boldsymbol{Y}_i^{\mathrm{H}}\right),\ \boldsymbol{H}_i^{\mathrm{Q}} = \frac{\mathrm{j}}{2}\left(\boldsymbol{Y}_i - \boldsymbol{Y}_i^{\mathrm{H}}\right) \tag{6a}$$

$$\boldsymbol{H}_{ij}^{\mathrm{P}} = \frac{1}{2}\left(\boldsymbol{Y}_{ij} + \boldsymbol{Y}_{ij}^{\mathrm{H}}\right),\ \boldsymbol{H}_{ij}^{\mathrm{Q}} = \frac{\mathrm{j}}{2}\left(\boldsymbol{Y}_{ij} - \boldsymbol{Y}_{ij}^{\mathrm{H}}\right) \tag{6b}$$

$$\boldsymbol{H}_i^{\mathrm{V}} = \boldsymbol{\xi}_i \boldsymbol{\xi}_i^{\mathrm{T}},\ \boldsymbol{H}_{ij}^{\mathrm{I}} = \frac{1}{2}\boldsymbol{Y}_{ij} \boldsymbol{Y}_{ij}^{\mathrm{H}} \tag{6c}$$

Based on the measurement matrices in (6), conventional measurements can be linearly represented by the voltage outer product. Distinct from the SCADA and AMI measurements, the novel high-precision D-PMU measurements are linearly related to the state variables. It is supposed that when a D-PMU is deployed at node i, the voltage phasor measurement at node i and the current phasor measurement of line $\mathcal{L}_{ij}$ connected with node i are available. Therefore, the measurement matrices of D-PMU can be expressed as follows.

$$\begin{aligned} \boldsymbol{H}_i^{\mathrm{PMU}} &= \boldsymbol{\Phi}_i^{\mathrm{H}} \boldsymbol{\Phi}_i \\ \boldsymbol{H}_{ij}^{\mathrm{PMU}} &= \boldsymbol{\Phi}_{ij}^{\mathrm{H}} \boldsymbol{\Phi}_{ij} \end{aligned} \tag{7}$$

where $\boldsymbol{\Phi}_i$ is the nodal voltage phasor measurement matrix related to node i, which is a diagonal matrix; $\boldsymbol{\Phi}_{ij}$ is the line current phasor measurement matrix related to line ij. $\boldsymbol{\Phi}_i$ and

$\boldsymbol{\Phi}_{ij}$ are both linearly related to the complex voltage state variables.

With the measurement matrices described above, the state estimation model considering the multi-source measurements in DDNs is transformed to the following equations [28].

$$f(\boldsymbol{\chi},\boldsymbol{V},\boldsymbol{v}) = \min_{\boldsymbol{\chi},\boldsymbol{V},\boldsymbol{v}} \sum_{n=1}^{S} \frac{1}{\sigma_n^2}\cdot \chi_n + \sum_{r=1}^{P} \frac{1}{\sigma_r^2}[\mathrm{Tr}(\boldsymbol{H}_r^{\mathrm{PMU}}\boldsymbol{V}) - 2\mathcal{R}(\boldsymbol{\zeta}_r^{\mathrm{H}}\boldsymbol{\Phi}_r\boldsymbol{v})] \tag{8a}$$

$$\text{s.t.} \begin{bmatrix} \chi_n & z_n - \mathrm{Tr}(\boldsymbol{H}_n\boldsymbol{V}) \\ z_n - \mathrm{Tr}(\boldsymbol{H}_n\boldsymbol{V}) & 1 \end{bmatrix} \succcurlyeq 0, \quad n = 1,\dots,S \tag{8b}$$

$$\mathrm{Tr}(\boldsymbol{H}_l\boldsymbol{V}) = 0, l = 1,\dots,Z \tag{8c}$$

$$\begin{bmatrix} \boldsymbol{V} & \boldsymbol{v} \\ \boldsymbol{v}^{\mathrm{H}} & 1 \end{bmatrix} \succcurlyeq 0 \tag{8d}$$

$$\mathrm{rank}(\boldsymbol{V}) = 1 \tag{8e}$$

where $\boldsymbol{H}_n$ and $\boldsymbol{H}_r^{\mathrm{PMU}}$ depend on the measurement type and are determined by (6) and (7), respectively; $\mathrm{rank}(\cdot)$ represents the rank of matrix "·"; $\mathcal{R}(\cdot)$ represents the real part of element "·"; $\boldsymbol{\chi}\epsilon\mathbb{R}^S$ is the auxiliary variable; constraint (8c) is the zero injection constraints; constraints (8d) and (8e) ensure that the voltage outer product is positive semidefinite and has a unique solution.

Due to the nonconvexity of rank-1 constraint (8e), it is usually relaxed when performing the convex state estimation problem. However, it is difficult to measure the voltage magnitude of all nodes in DDNs and the measurement accuracy varies significantly, only the high-rank solution $\boldsymbol{V}'$ can be obtained for (8). The voltage vector $\boldsymbol{v}$ can be recovered from the high-rank solution $\boldsymbol{V}'$ based on eigenvalue decomposition [24].

$$\boldsymbol{V}' = \sum_{\alpha=1}^{\omega} \lambda_\alpha \boldsymbol{v}_\alpha \boldsymbol{v}_\alpha^{\mathrm{H}} \tag{9}$$

where ω is the rank of $\boldsymbol{V}'$; λ_α and $\boldsymbol{v}_\alpha$ are the α-th eigenvalue and eigenvector, respectively. Select the largest eigenvector $\boldsymbol{v}_1$ as the rank-1 solution of (8), the estimated voltage satisfying the accuracy requirements can be obtained, which will be verified in Section IV.

III. PAC-Based Distributed State Estimation

Considering the digitization transformation of distribution networks, this section defines the control area of edge computing devices, then a distributed state estimation method based on the PAC algorithm is proposed. The consistency and convergence of estimation results in multiple areas are guaranteed by the interaction of boundary information.

A. Area Division with Edge Computing Devices

The edge computing devices in all areas integrate information collection, analysis, storage and calculation, which can be used for situation awareness of large-scale DDNs. A reasonable area division scheme can reduce computational complexity and communication burden of DDNs. Existing studies have proposed some methods for the area division of distribution networks [29], [30], which can be applied in this paper. Therefore, the area division of DDNs is not the focus of this paper, and the following assumptions are considered.

(as.1) The division of areas is based on the actual topology or geographical location. The number of nodes in each area shall be as consistent as possible, to minimize the total execution time of state estimation.

(as.2) The network $\{\mathcal{N},\mathcal{L}\}$ of each area has a tree topology.

(as.3) The adjacent areas are non overlapped and connected by lines. The parameters of these lines and the measurements on these lines are shared by adjacent areas.

To implement the proposed DSE method in DDNs, the following conditions need to be satisfied.

(cond.1) Each area contains only one edge computing device, which collects multi-source measurements from sensing terminals. The measurement configuration ensures the observability of each area.

(cond.2) The data interaction of adjacent edge computing devices is realized by reliable peer-to-peer communication, e.g. the wireless 5G networks, which satisfies the ever-increasing demands of maximizing throughput and minimizing latency.

The proposed method is carried out in a distributed manner without any control center. Measurements on the shared branches can be used to obtain the equivalent power injection of adjacent areas, which increases the measurement redundancy. In addition, the PAC algorithm interacts with boundary information including phase angle reference, which can achieve a consistent phase angle of the whole network. The next subsection will present the DSE method based on the PAC algorithm.

B. PAC-based DSE Method in DDNs

Based on the area division previously, consider a multi-area DDN $\{\mathcal{N},\mathcal{L}\}$ consisting of K edge computing devices. Suppose that S_k conventional measurements and P_k D-PMU measurements aggregated at area k are concatenated in $\boldsymbol{z}_k$, and obey the model (10).

$$\boldsymbol{z}_k = \boldsymbol{h}_k(\boldsymbol{v}_k) + \boldsymbol{e}_k \tag{10}$$

where $\boldsymbol{h}_k$ is the nonlinear measurement function of area k. Then the centralized SDP model (8) is recast to distributed form. The state estimation is carried out independently in each area, and only the state in the area is estimated. For any area k, the state estimation model is as follows.

$$f(\boldsymbol{\chi}_k,\boldsymbol{V}_k,\boldsymbol{v}_k) = \min_{\boldsymbol{\chi}_k,\boldsymbol{V}_k,\boldsymbol{v}_k} \sum_{n=1}^{S_k} \frac{1}{\sigma_{k,n}^2}\cdot \chi_{k,n} + \sum_{r=1}^{P_k} \frac{1}{\sigma_{k,r}^2}[\mathrm{Tr}(\boldsymbol{H}_{k,r}^{\mathrm{PMU}}\boldsymbol{V}_k) - 2\mathcal{R}(\boldsymbol{\zeta}_{k,r}^{\mathrm{H}}\boldsymbol{\Phi}_{k,r}\boldsymbol{v}_k)] \tag{11a}$$

$$\text{s.t.} \begin{bmatrix} \chi_{k,n} & z_{k,n} - \mathrm{Tr}(\boldsymbol{H}_{k,n}\boldsymbol{V}_k) \\ z_{k,n} - \mathrm{Tr}(\boldsymbol{H}_{k,n}\boldsymbol{V}_k) & 1 \end{bmatrix} \succcurlyeq 0, \quad n = 1,\dots,S_k \tag{11b}$$

$$\mathrm{Tr}(\boldsymbol{H}_{k,l}\boldsymbol{V}_k) = 0, l = 1,\dots,Z_k \tag{11c}$$

$$\begin{bmatrix} \boldsymbol{V}_k & \boldsymbol{v}_k \\ \boldsymbol{v}_k^{\mathrm{H}} & 1 \end{bmatrix} \succcurlyeq 0 \tag{11d}$$

$$\boldsymbol{V}_k = \overline{\boldsymbol{V}}_k \tag{11e}$$

where $\overline{\boldsymbol{V}}_k$ represents the voltage outer product of area k, and (11e) indicates that the voltage outer product of each area shall be consistent with the whole network.

However, the distributed state estimation model is not fully decomposed due to (11e). Specifically, there are measurements at boundary nodes and power coupling between adjacent areas. The atomic decomposition profile is adopted to render the problem decomposable, which is embodied in the following form.

$$\mathcal{D} = (L, C, S, O, T) \tag{12}$$

where:

$L = \{L_j, \forall j \in K\}$ represents the set of own atomic variables in each atom, that is, the state variables $\boldsymbol{V}_k$ of area k;

$C = \{C_j, \forall j \in K\}$ represents the set of constraints for each atom's own atomic variables, that is, the zero injection constraints of area k;

$S = \{S_j, \forall j \in K\}$ represents the objective function of each atom, that is, the objective function $\tilde{f}_k(\boldsymbol{V}'_k)$ of area k;

$O = \{O_j, \forall j \in K\}$ represents the external atomic variables of each atom, that is, the boundary information $\boldsymbol{V}_{k,l}$ of area k, and the corresponding rows and columns of the voltage outer product of area l adjacent to area k;

$T = \{T_j, \forall j \in K\}, T_j = L_j \cup O_j = \boldsymbol{V}'_k$ represents all optimization variables for each atom, that is, the equivalent state variables $\boldsymbol{V}'_k$ of area k (including state variables of this area and neighboring areas).

For the DDNs, each area k corresponds to an atom. Therefore, by using the atomic decomposition profile (12), the PAC algorithm decouples the global optimization into each atomic optimization. Based on the atomic partition described in (12), the atomized state estimation problem is formulated as follows.

$$\tilde{f}(\boldsymbol{V}'_k) = \min_{\boldsymbol{V}'_k} \tilde{f}_k(\boldsymbol{V}'_k) \tag{13a}$$

$$\text{s.t.}\ \widetilde{\boldsymbol{D}}_k \boldsymbol{V}'_k = \boldsymbol{0} \tag{13b}$$

$$\boldsymbol{J}_k \boldsymbol{V}'_k = \boldsymbol{0} \tag{13c}$$

where $\boldsymbol{V}'_k$ represents the atomic optimization variables including its own variables and external variables; $\tilde{f}_k(\boldsymbol{V}'_k)$ represents the objective function with respect to the atomic variables; equation (13b) represents the zero injection constraints (11c) and positive semidefinite constraints (11d) related to the voltage outer product; equation (13c) represents the boundary constraints (11e) of the voltage outer product.

Since the optimization variables in (13) is a matrix, the coordination constraint matrix $\boldsymbol{J}_k$ is extended to a three-dimensional tensor form. $\boldsymbol{J}_k$ is the incidence matrix represented by a directed graph, which represents the coordination between atoms and ensures the consistency of boundary solutions of each atom. Each row of $\boldsymbol{J}_k$ is the arrangement of all atomic variables of each atom, and each column is the arrangement of all external variables of each atom. The matrix elements are described as follows.

$$\boldsymbol{J}_{ij} = \begin{cases} -1, & \text{if } i \text{ is owned and } j \text{ is external} \\ 1, & \text{if } j \text{ is owned and } i \text{ is external} \\ 0, & \text{otherwise} \end{cases} \tag{14}$$

So far, the atomized DSE problem (13) has been modeled, and will be solved by the PAC algorithm. Firstly, each area forms a Lagrange function for

$$\mathcal{L}_k(\boldsymbol{V}'_k, \boldsymbol{\mu}_k, \boldsymbol{\nu}_k) = \tilde{f}_k(\boldsymbol{V}'_k) + \boldsymbol{\mu}_k^{\mathrm{T}} \widetilde{\boldsymbol{D}}_k \boldsymbol{V}'_k + \boldsymbol{\nu}_k^{\mathrm{T}} \boldsymbol{J}_k \boldsymbol{V}'_k \tag{15}$$

where $\boldsymbol{\mu}_k$, $\boldsymbol{\nu}_k$ are Lagrange multipliers corresponding to internal constraints and interval coordination constraints for area k, respectively. Adding l_2-regularization term and penalty term to $\boldsymbol{\mu}_k$ and $\boldsymbol{\nu}_k$, which is shown as follows.

$$\mathcal{L}_k(\boldsymbol{V}'_k, \widehat{\boldsymbol{\mu}}_k, \hat{\boldsymbol{\nu}}_k) = \tilde{f}_k(\boldsymbol{V}'_k) + \widehat{\boldsymbol{\mu}}_k^{\mathrm{T}} \widetilde{\boldsymbol{D}}_k \boldsymbol{V}'_k + \hat{\boldsymbol{\nu}}_k^{\mathrm{T}} \boldsymbol{J}_k \boldsymbol{V}'_k + \frac{1}{2\rho} ||\boldsymbol{V}'_k - \overline{\boldsymbol{V}}_k||_2^2 \tag{16}$$

where ρ is a constant step pre-allocated to all areas; $\overline{\boldsymbol{V}}_k$ is the theoretical optimum which is usually selected as the last iteration result; $\widehat{\boldsymbol{\mu}}_k$ and $\hat{\boldsymbol{\nu}}_k$ are Lagrange multipliers considering l_2-regularization constraints.

$$\begin{aligned} \widehat{\boldsymbol{\mu}}_k &= \boldsymbol{\mu}_k + \rho\gamma \widetilde{\boldsymbol{D}}_k \boldsymbol{V}'_k \\ \hat{\boldsymbol{\nu}}_k &= \boldsymbol{\nu}_k + \rho\gamma \boldsymbol{J}_k \boldsymbol{V}'_k \end{aligned} \tag{17}$$

Then apply the prox-linear approach of [31] to (16) and obtain the PAC-based DSE algorithm.

$$\boldsymbol{V}'_k[\tau+1] = \arg\min_{\boldsymbol{V}'_k} \{\mathcal{L}_k(\boldsymbol{V}'_k, \widehat{\boldsymbol{\mu}}_k[\tau], \hat{\boldsymbol{\nu}}_k[\tau])\} \tag{18}$$

$$\boldsymbol{\mu}_k[\tau+1] = \boldsymbol{\mu}_k[\tau] + \rho\gamma_k \widetilde{\boldsymbol{D}}_k \boldsymbol{V}'_k[\tau+1] \tag{19a}$$

$$\widehat{\boldsymbol{\mu}}_k[\tau+1] = \boldsymbol{\mu}_k[\tau+1] + \rho\hat{\gamma}_k[\tau+1] \widetilde{\boldsymbol{D}}_k \boldsymbol{V}'_k[\tau+1] \tag{19b}$$

$$\boldsymbol{\nu}_k[\tau+1] = \boldsymbol{\nu}_k[\tau] + \rho\gamma_k \boldsymbol{J}_k \boldsymbol{V}'_k[\tau+1] \tag{19c}$$

$$\hat{\boldsymbol{\nu}}_k[\tau+1] = \boldsymbol{\nu}_k[\tau+1] + \rho\hat{\gamma}_k[\tau+1] \boldsymbol{J}_k \boldsymbol{V}'_k[\tau+1] \tag{19d}$$

where γ_k is the over relaxation term of area k, which is time-varying in the update of dual variables $\widehat{\boldsymbol{\mu}}_k$ and $\hat{\boldsymbol{\nu}}_k$. The prox-linear approach is utilized to ensure parallel computation of primal steps (19a) and (19c).

The primal and dual variables are initialized according to the following equations.

$$\begin{aligned} \boldsymbol{\mu}_k[0] &= \rho\gamma_k \widetilde{\boldsymbol{D}}_k \boldsymbol{V}'_k[0] \\ \widehat{\boldsymbol{\mu}}_k[0] &= \boldsymbol{\mu}_k[0] + \rho\hat{\gamma}_k[0] \widetilde{\boldsymbol{D}}_k \boldsymbol{V}'_k[0] \\ \boldsymbol{\nu}_k[0] &= \rho\gamma_k \boldsymbol{J}_k \boldsymbol{V}'_k[0] \\ \hat{\boldsymbol{\nu}}_k[0] &= \boldsymbol{\nu}_k[0] + \rho\hat{\gamma}_k[0] \boldsymbol{J}_k \boldsymbol{V}'_k[0] \end{aligned} \tag{20}$$

C. Coordination of Edge Computing Devices

In DDNs, the edge computing devices need to communicate with the adjacent devices to achieve coordination. However, the objective function, constraints, measurements, and primal variables of the PAC algorithm are not shared among atoms, only a preserved dual variable $\hat{\boldsymbol{\nu}}_k$ is exchanged. The dual variable $\hat{\boldsymbol{\nu}}_k$ essentially contains the boundary information between atoms and realizes the uniform convergence of each area by the coordination matrix $\boldsymbol{J}_k$. The exchange of dual variable $\hat{\boldsymbol{\nu}}_k$ is for the following two reasons: a) $\hat{\boldsymbol{\nu}}_k$ contains the boundary information, which will be added in the Lagrange function (18) of the next PAC iteration together with the dual variable $\widehat{\boldsymbol{\mu}}_k$; b) $\hat{\boldsymbol{\nu}}_k$ is the "preserved" dual variable, which means each area cannot recover the "true" primal variable $\boldsymbol{\nu}_k$ through the "preserved" Lagrange multiplier $\hat{\boldsymbol{\nu}}_k$, and the same to the internal information $\boldsymbol{V}'_k$. This ensures the boundary constraints (13c) will work fairly and effectively.

The parameter iteration is illustrated in Fig. 2. It can be seen that each area firstly updates the Lagrange multiplier $\boldsymbol{\nu}_k$

according to (19c), then updates the Lagrange multiplier $\hat{\boldsymbol{v}}_k$ according to (19d) and broadcasts $\hat{\boldsymbol{v}}_k$ to all neighbors. The edge computing devices can adopt 5G communication networks which can have the data capacity of more than 1 Gb/s and support 1-ms latency, and reduce the communication delay greatly [32]. Since the interval of state estimation is usually at a minute level, the impact of the communication delay on state estimation can be negligible and the timeliness of state estimation will be guaranteed. Until all areas are updated, the new Lagrange multiplier $\hat{\boldsymbol{v}}_k$ is incorporated into the objective function (18) for the next optimization. The sublinear convergence of the PAC algorithm ensures that the voltage converges to the global optimum.

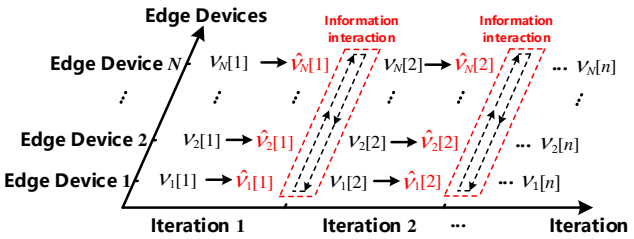

Fig. 2. Parameter iteration of the PAC-based DSE algorithm.

It can be seen that the iteration update structure in (19) exhibits symmetry between the primal and dual variables, which means the primal and dual variables $(\boldsymbol{\mu}_k, \hat{\boldsymbol{\mu}}_k)$ and $(\boldsymbol{v}_k, \hat{\boldsymbol{v}}_k)$ are updated simultaneously. The structure of parameter iteration is similar to the accelerated gradient method [33], where dual variables $\hat{\boldsymbol{\mu}}_k$ and $\hat{\boldsymbol{v}}_k$ are accelerated and the primal variables $\boldsymbol{\mu}_k$ and $\boldsymbol{v}_k$ are still in the usual way. Different from other algorithms, the PAC algorithm only needs to exchange dual variables and leads to a strictly sublinear convergence in iteration, which reduces the computational complexity. In addition, the primal variables cannot be recovered through the dual variables, which effectively realizes the privacy preserving and information security of edge computing devices.

D. Implementation of Distributed State Estimation

This subsection describes the procedures of deploying and implementing the PAC-based DSE algorithm on edge computing devices in detail. The flow chart of the proposed DSE method is shown in Fig. 3.

Firstly, each area contains only one edge computing device, and each edge computing device obtains the network topology parameters and multi-source measurements from sensing terminals. The topology analysis in the area is carried out to determine the state variables $\boldsymbol{V}_k'$. Then, the PAC-based DSE model (13) in DDNs is formulated. When finishing one-step optimization (18), the preserved boundary information $\hat{\boldsymbol{v}}_k$ is exchanged with the adjacent devices to update the state variables $\boldsymbol{V}_k'$. If the maximum voltage deviation among all areas is less than the convergence threshold, output the estimation results and the DSE is completed. If not, update the estimation parameters and the next-step optimization is carried out.

Note that the objective function (8a) is still a weighted least squares cost function. After solving the PAC-based DSE of each area, the well-developed method of bad data identification, such as the largest normalized residual method [34], can still be applied based on the analysis of measurement residuals. Some artificial intelligence methods, such as the generative adversarial networks [35], can also eliminate bad data before state estimation.

During the execution of the DSE in DDNs, the SDP model is used to ensure convergence in each area, and the PAC algorithm is utilized for coordination between areas. Based on the edge computing devices in DDNs, the proposed DSE realizes the accurate state perception and lays the foundation for advanced applications on the edge side of distribution networks.

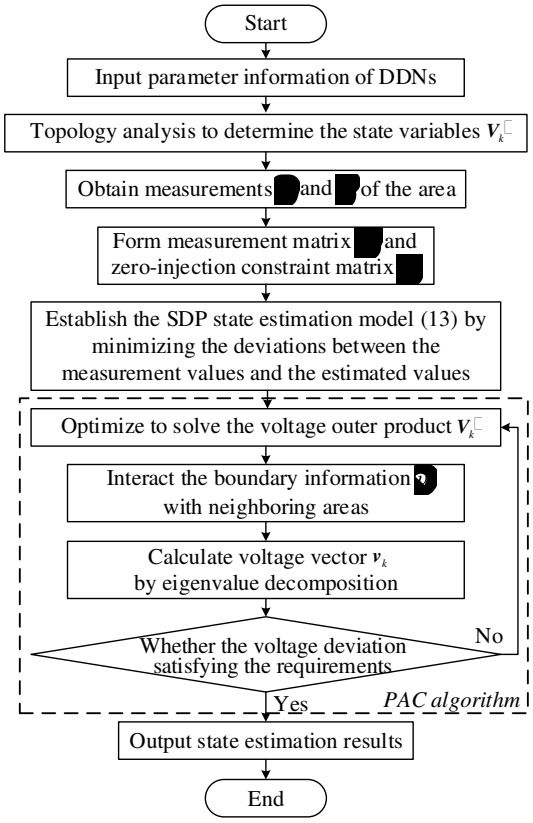

Fig. 3. Flow chart of the proposed distributed state estimation in DDNs.

IV. Case Studies and Analysis

In this section, the proposed DSE method is firstly tested on the modified PG&E 69-node system [36]. The system is divided into six areas according to the topology, that is, six edge computing devices are deployed. Different area divisions will not affect the applicability of the proposed method. The topology, sensing terminals configuration, and areas are shown in Fig. 4. The system consists of 68 lines with a rated voltage level of 12.66 kV. The total active power and reactive power demands are 3715 kW and 2300 kVAr, respectively. Ten PVs are integrated at nodes 3, 14, 19, 27, 34, 38, 43, 49, 55 and 62, whose capacity is 300 kWp. Each area contains at least one DG and the penetration of DG reaches 80%. All load nodes are monitored with AMI measurements, and some nodes and lines are monitored with SCADA and D-PMU measurements. In addition, the system contains 20 zero injection nodes. The true value is simulated based on OpenDSS [37], and the measurement value is generated by adding the random measure-

ment noise of Gaussian distribution to the real value. The measurement noise standard deviations of AMI, SCADA, and D-PMU are 5%, 1%, and 0.1%, respectively. D-PMUs are installed to improve the measurement redundancy and monitor important nodes.

To verify the effectiveness of the proposed method in this paper, the solution (Scheme V) is compared with other four methods (Schemes I – IV), which are described as follows:

Scheme I: the true value is obtained from OpenDSS;

Scheme II: the traditional Gauss-Newton method is utilized to solve the centralized state estimation in DDNs;

Scheme III: the SDP method in Section II is utilized to solve the centralized state estimation in DDNs;

Scheme IV: the SDP-based ADMM method in Ref. [28] is utilized to solve the distributed state estimation in DDNs;

Scheme V: the SDP-based PAC method in Section III is utilized to solve the distributed state estimation in DDNs.

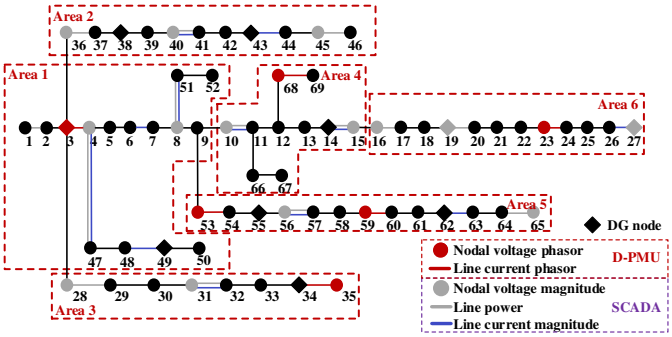

Fig. 4. Structure of the modified PG&E 69-node system.

The proposed method is implemented in MATLAB R2020a. All numerical experiments are carried out with SDPT3 4.0 solver [38] in CVX [39] on an Intel Core i7 @ 3.20GHz desktop with 16GB RAM.

A. Convergence Analysis

To evaluate the convergence of the proposed DSE method, 100 tests are carried out in four schemes. Table I gives the comparison of the convergence ratio. The definition of convergence is that the iterations are less than 50 times under a given convergence threshold. For example, the second and third columns in the table are the convergence times of the Gauss-Newton method with the threshold of 1×10^{-5} and 1×10^{-6}, respectively, and there are 92 and 78 times of convergence in 100 tests, respectively.

TABLE I

COMPARISON OF CONVERGENCE FOR THE PG&E 69-NODE SYSTEM

Scheme	Scheme II		Scheme III	Scheme IV		Scheme V	
ε	1×10^{-5}	1×10^{-6}	-	1×10^{-5}	1×10^{-6}	1×10^{-5}	1×10^{-6}
Convergence Ratio(%)	92	78	100	100	100	100	100

It can be seen that in Scheme II there are 8 times of non-convergence with the convergence threshold of 1×10^{-5} and 22 times with the convergence threshold of 1×10^{-6}. When solving the centralized state estimation with the Gauss-Newton method, the load level at Node 61 is much heavier than that of other nodes. The gain matrix appears "ill-conditioned", and the numerical stability is reduced, resulting in the non-convergence of the iteration. Distinct from Scheme II, the converged scenarios in Scheme III means that the gap between the primal and dual objectives falls within the threshold of 1×10^{-8}. The results in Scheme III indicate that by solving the convex optimization of (8), the SDP method obtains feasible solutions without convergence problem. Simlarly, there is also no convergence problem in Scheme IV and V, which fully illustrates the effectiveness of the proposed DSE method, and supports the operation and regulation of DDNs.

B. Accuracy Analysis

The estimation accuracy of all nodes in all areas is evaluated. The solution of the estimation accuracy in Schemes II, III, IV, and V is compared. Two indices are selected for the estimation accuracy analysis.

$$\begin{aligned}\text{Magnitude Error (ME)} &= \frac{|V_{\text{se}}-V_{\text{true}}|}{V_{\text{true}}}\times 100\% \\ \text{Phase Angle Error (PAE)} &= |\theta_{\text{se}}-\theta_{\text{true}}|\end{aligned} \tag{21}$$

Table II and Fig. 5 show the average estimation error of voltage magnitude and phase angle. It can be seen from Table II that the centralized state estimation in Scheme II has the highest estimation accuracy, that is, the smallest voltage magnitude and phase angle error. Scheme III obtains the second-highest estimation accuracy; the decrease in the estimation accuracy results from the rank-1 constraint relaxation and the eigenvalue decomposition of the high-rank solution in comparison with Scheme II. Ref. [24] can further improve the accuracy through the convex iterative method, but it will bring a massive computational burden.

TABLE II

COMPARISON OF STATE ESTIMATION ERRORS FOR THE PG&E 69-NODE SYSTEM

Area	Index	Scheme II	Scheme III	Scheme IV	Scheme V
1	Average ME(%)	0.0075	0.0795	0.1342	0.1097
	Average PAE(°)	0.0008	0.0017	0.0044	0.0029
2	Average ME(%)	0.0082	0.0751	0.1251	0.1051
	Average PAE(°)	0.0009	0.0004	0.0053	0.0030
3	Average ME(%)	0.0088	0.0735	0.1234	0.1034
	Average PAE(°)	0.0004	0.0002	0.0008	0.0003
4	Average ME(%)	0.0067	0.0914	0.1425	0.1221
	Average PAE(°)	0.0017	0.0125	0.0165	0.0145
5	Average ME(%)	0.0140	0.1209	0.1762	0.1564
	Average PAE(°)	0.0021	0.0057	0.0097	0.0077
6	Average ME(%)	0.0048	0.0669	0.1181	0.0976
	Average PAE(°)	0.0045	0.0254	0.0294	0.0274

Distributed methods in Scheme IV and V cannot achieve the accuracy of centralized methods naturally. The cost of parallelization is the addition of coordination constraints to be satisfied for each area, which ensures global consistency and the error between areas is unavoidable for distributed algorithms. The estimation accuracy of Scheme V is slightly worse than

that of Scheme III, which is mainly caused by the consistency constraints between areas. Scheme IV has the worst estimation accuracy. The estimation accuracy of distributed methods is less than that of centralized methods.

However, compared with the ADMM-based method in Scheme IV, the PAC-based method in Scheme V reflects the advantages in estimation accuracy, which can provide more accurate operating states for advanced applications. The average estimation errors of nodal voltage magnitude in Scheme V are less than 0.5%, which meets the accuracy requirements of practical applications.

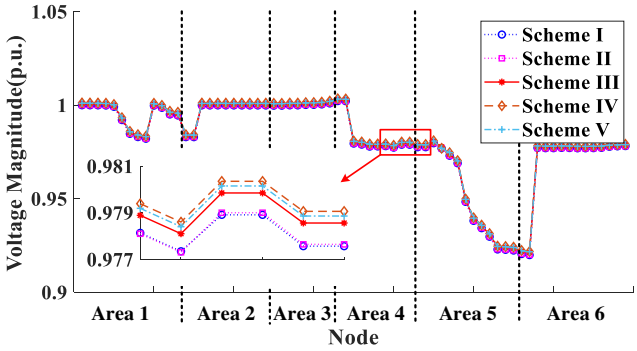

(a) Comparison of nodal voltage magnitude.

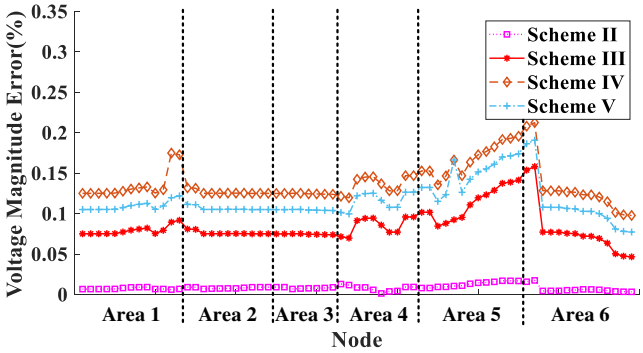

(b) Comparison of estimation errors of nodal voltage magnitude.

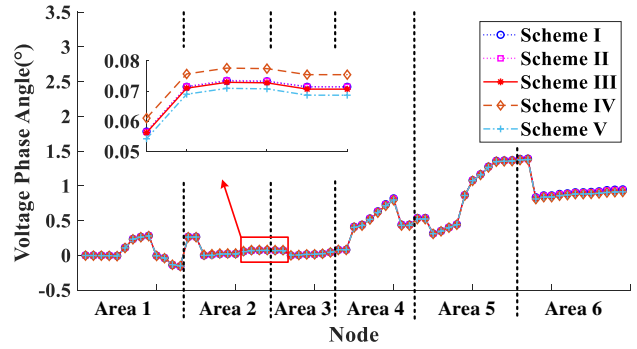

(c) Comparison of nodal voltage phase angle.

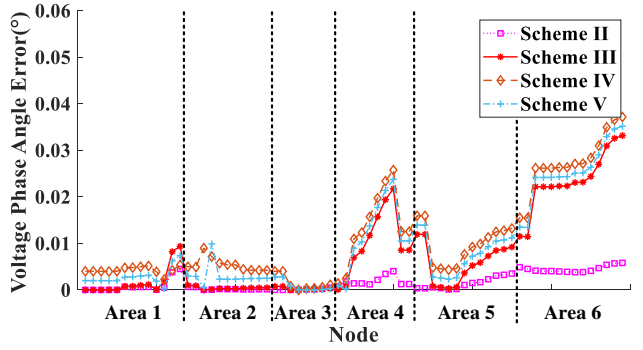

(d) Comparison of estimation errors of nodal voltage phase angle.

Fig. 5. Comparison of state estimation results for the PG&E 69-node system.

Fig. 6 shows the comparison of iteration error at Node 9. Node 9 is the boundary node of Area 1. The results show that the PAC algorithm slightly outperforms the ADMM algorithm on the consistency metric by achieving a lower error, while both are comparable in the feasibility metric.

C. Computational Efficiency Analysis

The rapid variation in the operating state of DDNs resulting from the variability and uncertainty of DGs puts forward higher requirements for the computation time of state estimation. To test the computation time of the proposed DSE method, the edge computing devices are simulated on the upper computer, which will be further tested on the actual edge computing devices in the future. Table III lists the computation time of state estimation with different schemes.

In particular, this paper does not consider the impact of communication delay of each edge computing device, and the computation time only includes optimization time for edge computing devices. The SDP method in Scheme III, which takes 16.7756s, is the most time-consuming due to solving the large-scale complex variable matrix. The computation time will further increase in larger-scale DDNs. In Scheme IV and V, each area performs state estimation independently, and the computation time is determined by the area that takes the longest time, which greatly reduces the computation time. In Scheme V, since Area 1 has more nodes than other areas, Area 1 takes the longest computation time (2.1826s) compared to all other areas. Other areas have the same scale and the computation time is close to each other. It can be seen from Table III that the computation time of the proposed DSE method is reduced from 16.7756s to 2.1826s, which greatly improves the computational efficiency of state estimation. In addition, due to the sublinear convergence, the PAC algorithm has superior iteration complexity. As can be seen from Fig. 6, the PAC algorithm converges after 10 iterations, while the ADMM algorithm converges after 13 iterations, which shows that the PAC algorithm has more advantages in convergence. The proposed method shows the potential for deployment in edge computing devices and reduces the computational burden.

TABLE III

COMPARISON OF COMPUTATION TIME FOR THE PG&E 69-NODE SYSTEM

	Area	Scheme III	Scheme IV	Scheme V
Computation time	Area 1	16.7756s	2.3590s	2.1826s
	Area 2		1.7369s	1.3263s
	Area 3		1.3494s	1.0548s
	Area 4		1.6512s	1.1593s
	Area 5		1.8309s	1.5421s
	Area 6		1.5907s	1.3427s

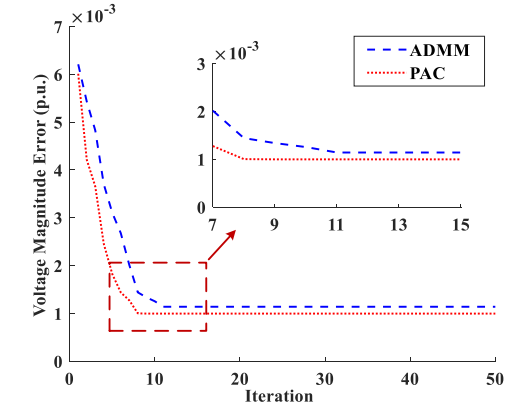

(a) Voltage magnitude error at Node 9.

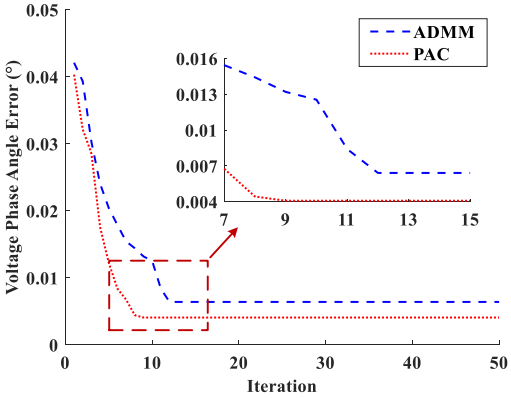

(b) Voltage phase angle error at Node 9.

Fig. 6. Comparison of iteration error at Node 9.

D. Adaptability Analysis

To illustrate the feasibility of the DSE in DDNs, the case from a practical pilot in Guangzhou, China is adopted. It is assumed that three edge computing devices are deployed in the system, which is determined by the geographical location. The system consists of 52 lines, with a rated voltage level of 10 kV, and the total active power and reactive power demands are 8790 kW and 1786 kVAr, respectively. The topology, sensing terminals configuration, and areas are shown in Fig. 7. The measurement values generated by simulation and scheme settings are similar to those in the previous subsection, which are not illustrated here.

Table IV shows the state estimation results of the practical pilot in Guangzhou. Different from the PG&E 69-node system, the load of this system is at the same level, thus there is no convergence problem in all four schemes. As it can be observed, Scheme II still maintains the minimum estimation error, and Scheme III remains at the same level, which is similar to the previous tests. The estimation error of Scheme V is less than that of Scheme IV. For the estimation results of all areas, Area 2 provides the best local estimation as it has relatively more voltage magnitude measurements, which improves the estimation accuracy of distributed state estimation. With the increased number of multi-source measurements, the benefits of the proposed DSE method will be significantly enhanced. In addition, when a certain area needs more accurate monitoring (including DGs, for example), it is necessary to improve the measurement redundancy of this area, which will reduce the total configuration cost. The proposed DSE method provides a promising solution to the state perception in the digitalized transformation of DDNs.

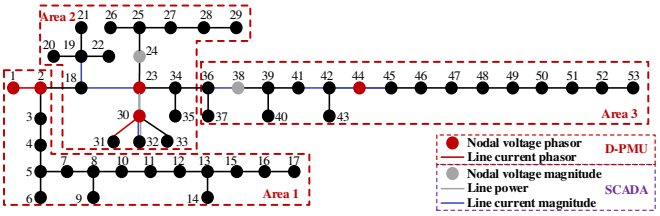

Fig. 7. Structure of the practical pilot in Guangzhou

TABLE IV

COMPARISON OF STATE ESTIMATION ERRORS FOR THE PRACTICAL PILOT IN GUANGZHOU

Area	Index	Scheme II	Scheme III	Scheme IV	Scheme V
1	Average ME(%)	0.1437	0.1729	0.2486	0.2253
	Average PAE(°)	0.0048	0.0239	0.0294	0.0282
2	Average ME(%)	0.0622	0.1312	0.3014	0.2120
	Average PAE(°)	0.0023	0.0086	0.0140	0.0130
3	Average ME(%)	0.3456	0.4906	0.4397	0.4396
	Average PAE(°)	0.0098	0.1122	0.1183	0.1172

V. CONCLUSIONS

With the development of digital technologies, the number of edge computing devices promotes the intelligent and digitalized transformation of distribution networks. The introduction of edge computing devices makes the multi-area state estimation possible in DDNs. Aiming at the convergence and computational efficiency in state perception of multi-area DDNs, this paper proposes a DSE method based on the PAC algorithm. In each area, the state estimation model is converted into an SDP model with convex relaxation technology, which solves the nonconvexity caused by nonlinear measurements. By interacting boundary information with neighbors, the coordination of state estimation among multiple areas is realized. The case studies and analysis are carried out on the modified PG&E 69-node system and the test case from a practical pilot in Guangzhou, China. The effective solution of state estimation is realized on the edge side, which improves the state perception ability of DDNs, and lays foundations for advanced application requirements. In the future, to further deal with the uncertainty and volatility of DGs, the massive historical measurement data will be considered. One of the extensions is to establish a data-driven based state estimation model to enhance the real-time situation awareness of multi-area DDNs.

REFERENCES

[1] Z. Tao *et al.*, "A survey of virtual machine management in edge computing," *Proc. IEEE*, vol. 107, no. 8, pp. 1482-1499, Aug. 2019.

[2] D. Della Giustina, M. Pau, P. A. Pegoraro, F. Ponci and S. Sulis, "Electrical distribution system state estimation: Measurement issues and challenges," *IEEE Trans. Instrum. Meas.*, vol. 17, no. 6, pp. 36-42, Dec. 2014.

[3] Y. Liu, M. Peng, G. Shou, Y. Chen and S. Chen, "Toward edge intelligence: Multiaccess edge computing for 5G and Internet of Things," *IEEE Internet Things J.*, vol. 7, no. 8, pp. 6722-6747, Aug. 2020.

[4] C. Feng, Y. Wang, Q. Chen, Y. Ding, G. Strbac and C. Kang, "Smart grid encounters edge computing: Opportunities and applications," *Adv. Appl. Energy*, vol. 1, Feb. 2021, Art. no. 100006.

[5] M. Mao, J. Xu, Z. Wu, Q. Hu and X. Dou, "A multiarea state estimation for distribution networks under mixed measurement environment," *IEEE Trans. Ind. Informat.*, vol. 18, no. 6, pp. 3620-3629, Jun. 2022.

[6] V. K. Singh, B. V. Suryakiran, A. Verma and T. S. Bhatti, "Modelling of a renewable energy-based AC interconnected rural microgrid system for the provision of uninterrupted power supply," *IET Energy Syst. Integr.*, vol. 3, no. 2, pp. 172-183, Jun. 2021.

[7] R. Ferrero, P. A. Pegoraro and S. Toscani, "Dynamic synchrophasor estimation by extended kalman filter," *IEEE Trans. Instrum. Meas.*, vol. 69, no. 7, pp. 4818-4826, Jul. 2020.

[8] P. Castello, R. Ferrero, P. A. Pegoraro and S. Toscani, "Effect of unbalance on positive-sequence synchrophasor, frequency, and ROCOF estimations," *IEEE Trans. Instrum. Meas.*, vol. 67, no. 5, pp. 1036-1046, May 2018.

[9] C. Dang, X. Wang, C. Shao and X. Wang, "Distributed generation planning for diversified participants in demand response to promote renewable energy integration," *J. Modern Power Syst. Clean Energy*, vol. 7, no. 6, pp. 1559-1572, Nov. 2019.

[10] Y. Huo *et al.*, "Data-driven adaptive operation of soft open points in active distribution networks," *IEEE Trans. Ind. Informat.*, vol. 17, no. 12, pp. 8230-8242, Dec. 2021.

[11] F. Aminifar, M. Shahidehpour, M. Fotuhi-Firuzabad and S. Kamalinia, "Power system dynamic state estimation with synchronized phasor measurements," *IEEE Trans. Instrum. Meas.*, vol. 63, no. 2, pp. 352-363, Feb. 2014.

[12] L. De Alvaro Garcia and S. Grenard, "Scalable distribution state estimation approach for distribution management systems," *2011 2nd IEEE PES International Conference and Exhibition on Innovative Smart Grid Technologies* (*ISGT*), pp. 1-6, Dec. 2011.

[13] A. Gomez-Exposito and A. de la Villa Jaen, "Two-level state estimation with local measurement pre-processing," *IEEE Trans. Power Syst.*, vol. 24, no. 2, pp. 676-684, May 2009.

[14] V. Kekatos and G. B. Giannakis, "Distributed robust power system state estimation," *IEEE Trans. Power Syst.*, vol. 28, no. 2, pp. 1617-1626, May 2013.

[15] S. Kar, G. Hug, J. Mohammadi, and J. M. Moura, "Distributed state estimation and energy management in smart grids: A consensus innovations approach," *IEEE J. Sel. Topics Signal Process.*, vol. 8, no. 6, pp. 1022-1038, Dec. 2014.

[16] X. Zhou, Z. Liu, Y. Guo, C. Zhao, J. Huang and L. Chen, "Gradient-based multi-area distribution system state estimation," *IEEE Trans. Smart Grid*, vol. 11, no. 6, pp. 5325-5338, Nov. 2020.

[17] M. Pau, F. Ponci, A. Monti, S. Sulis, C. Muscas and P. A. Pegoraro, "An efficient and accurate solution for distribution system state estimation with multiarea architecture," *IEEE Trans. Instrum. Meas.*, vol. 66, no. 5, pp. 910-919, May 2017.

[18] N. Nusrat, P. Lopatka, M. R. Irving, G. A. Taylor, S. Salvini and D. C. H. Wallom, "An overlapping zone-based state estimation method for distribution systems," *IEEE Trans. Smart Grid*, vol. 6, no. 4, pp. 2126-2133, Jul. 2015.

[19] Y. Chen, J. Ma, P. Zhang, F. Liu and S. Mei, "Robust state estimator based on maximum exponential absolute value," *IEEE Trans. Smart Grid*, vol. 8, no. 4, pp. 1537-1544, Jul. 2017.

[20] J. Zhao, L. Mili and R. C. Pires, "Statistical and numerical robust state estimator for heavily loaded power systems," *IEEE Trans. Power Syst.*, vol. 33, no. 6, pp. 6904-6914, Nov. 2018.

[21] F. V. Lima, M. R. Rajamani, T. A. Soderstrom and J. B. Rawlings, "Covariance and state estimation of weakly observable systems: Application to polymerization processes," *IEEE Trans. Control Syst. Technol.*, vol. 21, no. 4, pp. 1249-1257, Jul. 2013.

[22] J. J. Romvary, G. Ferro, R. Haider and A. M. Annaswamy, "A proximal atomic coordination algorithm for distributed optimization," *IEEE Trans. Autom. Control*, vol. 67, no. 2, pp. 646-661, Feb. 2022.

[23] R. Haider, S. Baros, Y. Wasa, J. Romvary, K. Uchida and A. M. Annaswamy, "Toward a retail market for distribution grids," *IEEE Trans. Smart Grid*, vol. 11, no. 6, pp. 4891-4905, Nov. 2020.

[24] Y. Yao, X. Liu, D. Zhao and Z. Li, "Distribution system state estimation: A semidefinite programming approach," *IEEE Trans. Smart Grid*, vol. 10, no. 4, pp. 4369-4378, Jul. 2019.

[25] Y. Liu, Z. Li, Q. H. Wu and H. Zhang, "Real-time dispatchable region of renewable generation constrained by reactive power and voltage profiles in AC power networks," *CSEE J. Power Energy Syst.*, vol. 6, no. 3, pp. 528-536, Sep. 2020.

[26] A. K. Ghosh, D. L. Lubkeman, M. J. Downey and R. H. Jones, "Distribution circuit state estimation using a probabilistic approach," *IEEE Trans. Power Syst.*, vol. 12, no. 1, pp. 45-51, Feb. 1997.

[27] A. S. Zamzam, X. Fu, and N. D. Sidiropoulos, "Data-driven learning-based optimization for distribution system state estimation," *IEEE Trans. Power Syst.*, vol. 34, no. 6, pp. 4796-4805, Nov. 2019.

[28] H. Zhu and G. B. Giannakis, "Power system nonlinear state estimation using distributed semidefinite programming," *IEEE J. Sel. Topics Signal Process.*, vol. 8, no. 6, pp. 1039-1050, Dec. 2014.

[29] Z. Zhao *et al.*, "Optimal placement of PMUs and communication links for distributed state estimation in distribution networks," *Appl. Energy*, vol. 256, Dec. 2019, Art. no. 113963.

[30] C. Muscas, M. Pau, P. A. Pegoraro, S. Sulis, F. Ponci and A. Monti, "Multiarea distribution system state estimation," *IEEE Trans. Instrum. Meas.*, vol. 64, no. 5, pp. 1140-1148, May 2015.

[31] G. Chen and M. Teboulle, "A proximal-based decomposition method for convex minimization problems", *Math. Progr.*, vol. 64, pp. 81-101, Mar. 1994.

[32] L. Lin, X. Liao, H. Jin and P. Li, "Computation offloading toward edge computing," *Proc. IEEE*, vol. 107, no. 8, pp. 1584-1607, Aug. 2019.

[33] M. I. Florea and S. A. Vorobyov, "An accelerated composite gradient method for large-scale composite objective problems," *IEEE Trans. Signal Process.*, vol. 67, no. 2, pp. 444-459, Jan. 2019.

[34] A. Abur and A. G. Exposito, *Power System State Estimation: Theory and Implementation*. Boca Raton, FL, USA: CRC Press, 2004.

[35] Y. Li, Y. Wang and S. Hu, "Online generative adversary network based measurement recovery in false data injection attacks: A cyber-physical approach," *IEEE Trans. Ind. Informat.*, vol. 16, no. 3, pp. 2031-2043, Mar. 2020.

[36] M. E. Baran and F. F. Wu, "Optimal capacitor placement on radial distribution systems," *IEEE Trans. Power Del.*, vol. 4, no. 1, pp. 725-734, Jan. 1989.

[37] R. C. Dugan, *Reference Guide for The Open Distribution System Simulator (OpenDSS)*, Elect. Power Res. Inst., Palo Alto, CA, USA, 2016.

[38] R. H. Tütüncü, K. C. Toh and M. J. Todd, "Solving semidefinite-quadratic-linear programs using SDPT3," *Math. Program.*, vol. 95, no. 2, pp. 189-217, Feb. 2003.

[39] M. Grant and S. Boyd, "CVX: Matlab software for disciplined convex programming," Apr. 2011, [Online]. Available: http://cvxr.com/cvx/.